



# Antiferromagnet-induced perpendicular magnetic anisotropy in ferromagnetic Co/Fe films with strong in-plane magnetic anisotropy

Bo-Yao Wang <sup>1,\*</sup>, Jing-Yu Ning,<sup>1</sup> Tzu-Hsin Li,<sup>1</sup> Chun-Chieh Chung,<sup>1</sup> Chun-Yao Hsu,<sup>1</sup> Ming-Shian Tsai,<sup>1,2</sup> Tzu-Hung Chuang <sup>3</sup>, and Der-Hsin Wei<sup>3</sup>

<sup>1</sup>*Department of Physics, National Changhua University of Education, Changhua 500, Taiwan*

<sup>2</sup>*Institute of Photonics Technologies, National Tsing Hua University, Hsinchu 300, Taiwan*

<sup>3</sup>*National Synchrotron Radiation Research Center, Hsinchu 300, Taiwan*



(Received 3 January 2022; revised 2 May 2022; accepted 3 May 2022; published 13 May 2022)

Ferromagnetic (FM) films with higher magnetic moment density typically exhibit sizable in-plane magnetic anisotropy as a result of strong dipolar interactions, which hinder their application in state-of-the-art perpendicularly based magnetic devices. This study reports the effects of triggering the perpendicular magnetic anisotropy (PMA) of a Co/Fe film with strong in-plane magnetic anisotropy through nearby antiferromagnetic (AFM) fcc Fe<sub>50</sub>Mn<sub>50</sub> and face-centered tetragonal (e-fct) Mn films. Our results demonstrate that fcc Fe<sub>50</sub>Mn<sub>50</sub> films with a three-dimensional quadratic AFM spin structure can trigger robust PMA in a Co/Fe film through collinearlike AFM-FM exchange coupling at room temperature. Furthermore, by incorporating a monolayered Fe<sub>50</sub>Mn<sub>50</sub> film into the Mn-Co interface or by reducing the temperature, PMA can also be triggered in a Co/Fe film by using e-fct Mn films with an in-plane-oriented AFM spin structure at room or low temperature through noncollinear exchange coupling across the AFM-FM interface. Our results clarify the exchange-coupling mechanisms, characteristic behaviors, and critical conditions for increasing control over antiferromagnet-induced PMA in FM films with high magnetic moment density but strong in-plane magnetic anisotropy, which is helpful for the development of next-generation perpendicularly based spintronic devices.

DOI: [10.1103/PhysRevB.105.184415](https://doi.org/10.1103/PhysRevB.105.184415)

## I. INTRODUCTION

Magnetic thin films exhibiting perpendicular magnetic anisotropy (PMA) have attracted considerable interest in the field of magnetism research because of their applicability in modern spintronic devices [1–4]. In general, ferromagnetic (FM) films with high magnetic moment density or spin polarization, such as Fe and Co layers, typically have strong in-plane magnetic anisotropy as a result of considerable dipolar interactions among the magnetic moments. Whereas FM/noble-metal multilayers with enhanced orbital hybridization at the interface [5,6] or tetragonal FM alloy films with asymmetric spin-orbit coupling (SOC) within the material [7,8] are conventional structures capable of exhibiting PMA. However, current control of PMA induction is limited to applications of SOC with a limited energy scale (approximately 10<sup>-2</sup> to 10<sup>-1</sup> eV/atom) [9]. Alternative methods are urgently needed to better control the PMA induction of FM films that exhibit high magnetic moment density and strong in-plane magnetic anisotropy.

Antiferromagnetic (AFM) thin films with various spin structures are another promising material for controlling the magnetic anisotropy of FM films through proximity effects and exchange coupling [10–16]. The strength of PMA induced by the adjacent AFM film is subject to the finite-size effect [17] and is usually affected by the thickness of the AFM film. Therefore, the incorporation of exchange coupling

with a higher energy scale (approximately 10<sup>-1</sup> to several eV/atom) [9] can provide more degrees of freedom in controlling PMA induction than SOC can alone [5–8]. AFM fcc Fe<sub>50</sub>Mn<sub>50</sub> films and vertically expanded face-centered tetragonal (e-fct) Mn films, which have a three-dimensional quadratic-type (3Q-type) [18–21] and a two-dimensional layered spin structure [22,23], respectively, can trigger PMA in a Co/Ni film [15,16,24]. However, studies have yet to examine these effects in Co/Fe-based FM films, which have a much higher magnetic moment density and stronger in-plane magnetic anisotropy [25].

In this paper, we present the effects of triggering PMA in an in-plane magnetic 3-monolayer (ML) Co/3-ML Fe film by applying AFM fcc Fe<sub>50</sub>Mn<sub>50</sub> and e-fct Mn films; the in-plane magnetic anisotropy energy of the 3-ML Co/3-ML Fe film ( $\approx -1.4$  mJ/m<sup>2</sup>) [25,26] (see also Supplemental Material [27] and Refs. [28–30]) is much higher than that of a 2-ML Co/14-ML Ni film ( $\approx -0.64$  mJ/m<sup>2</sup>) used in previous reports [15,16,24,31] and of a 6-ML (1.2 nm) CoFeB alloy film ( $\approx -0.9$  mJ/m<sup>2</sup>) [1] typically used in perpendicular-based spin-transfer torque devices. Our results indicate that robust PMA of a 3-ML Co/3-ML Fe film can be triggered by a fcc Fe<sub>50</sub>Mn<sub>50</sub> film with a three-dimensional quadratic AFM spin structure through collinearlike AFM-FM exchange coupling at room temperature. In addition, if a monolayered Fe<sub>50</sub>Mn<sub>50</sub> film is incorporated into the Mn-Co interface or the temperature is reduced, the PMA of a Co/Fe film can also be triggered by e-fct Mn films with an in-plane-oriented AFM spin structure at room or low temperature through noncollinear exchange coupling across the AFM-FM

\*bywang1735@cc.ncue.edu.tw

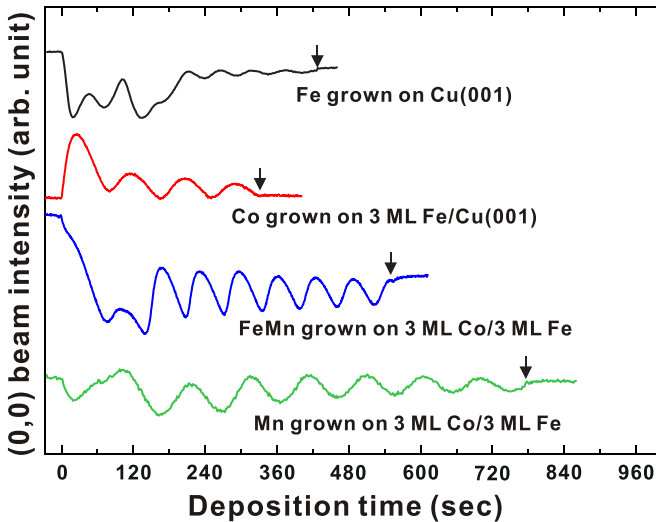


FIG. 1. Selected MEED (0,0) beam intensity curves as a function of deposition time for Fe film grown on Cu(001), Co film grown on 3-ML Fe/Cu(001), and Fe<sub>50</sub>Mn<sub>50</sub> and Mn films grown on 3-ML Co/3-ML Fe/Cu(001) at 300 K. Film thickness was calibrated by the oscillations in the MEED curves. The arrows indicate the time for the shutter to be closed.

interface. Our results clarify the exchange-coupling mechanisms, characteristic behaviors, and critical conditions for increasing control over antiferromagnet-induced PMA in FM films with a higher magnetic moment density but stronger in-plane magnetic anisotropy.

## II. EXPERIMENT

In this study, the growth condition, crystalline structure, and magnetic properties of a series of Fe<sub>50</sub>Mn<sub>50</sub>(Mn)/3-ML

Co/3-ML Fe films were investigated *in situ* in a multifunctional ultra-high-vacuum chamber with a base pressure of  $2 \times 10^{-10}$  torr. Single crystalline Cu(001) substrates with a well-ordered crystalline structure and smooth surfaces were prepared through cycles of 2-keV Ar<sup>+</sup> ion sputtering and subsequent annealing at 800 K for 5 min. All films were deposited at room temperature by using an electron gun (e-beam evaporator) with a flux monitor. After a 3-ML Co/3-ML Fe film was deposited on Cu(001), a series of Fe<sub>50</sub>Mn<sub>50</sub>(Mn)-based AFM films, namely, Fe<sub>50</sub>Mn<sub>50</sub>, Mn, and Mn/1-ML Fe<sub>50</sub>Mn<sub>50</sub> films, were prepared on 3-ML Co/3-ML Fe/Cu(001). The deposition rates and thicknesses of the films were monitored using medium-energy electron diffraction (MEED). Figure 1 illustrates the typical specular MEED (0,0) beam intensity of the Fe films grown on Cu(001), Co films grown on 3-ML Fe/Cu(001), and Fe<sub>50</sub>Mn<sub>50</sub> or Mn films grown on 3-ML Co/3-ML Fe/Cu(001). Regular oscillation indicates layer-by-layer growth conditions for these films. The average in-plane and vertical interlayer distances of the films were measured *in situ* using low-energy electron diffraction (LEED) with a kinematic approximation (LEED *I/V*). The magnetic hysteresis loops of the samples were measured *in situ* using magneto-optical Kerr effects (MOKE) in both the longitudinal and polar geometries. Temperature-dependent MOKE measurements were performed from 155 to 300 K. The characteristic interface couplings of the individual magnetic elements in the Fe<sub>50</sub>Mn<sub>50</sub>(Mn)/3-ML Co/3-ML Fe films in which PMA was established were also detected *in situ* by assessing the x-ray magnetic circular dichroism (XMCD) effects [9] measured at the Mn, Fe, and Co *L*<sub>3,2</sub> absorption edges in total electron yield mode. These measurements were performed in an x-ray photoemission electron microscopy (PEEM) [32–34] end station at beamline BL05B2 of the Taiwan Light Source at the National Synchrotron Radiation Research Center. The measurements of the x-ray absorption spectrum (XAS) and XMCD curves

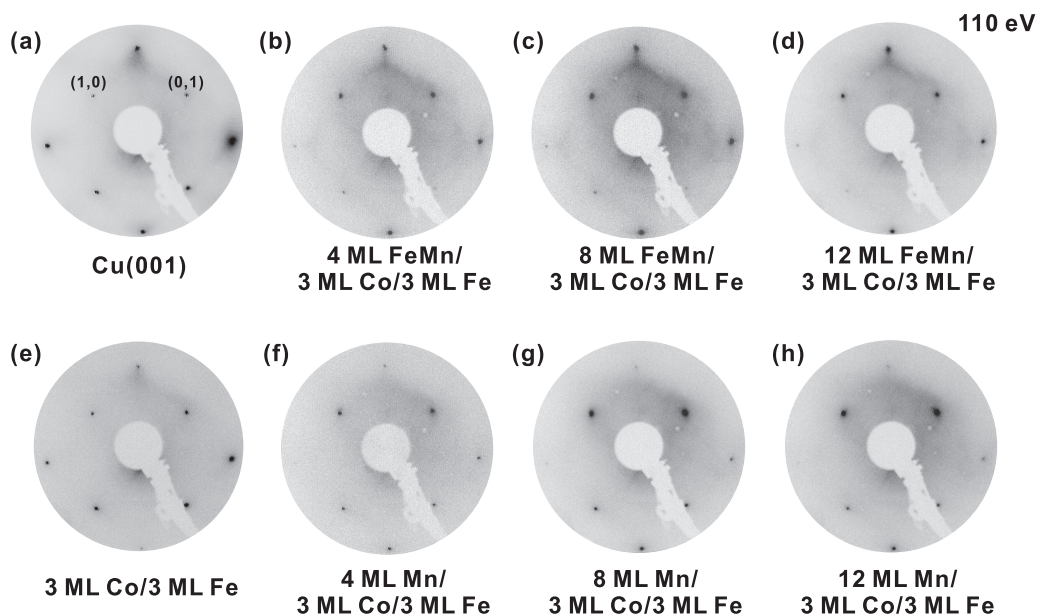


FIG. 2. LEED patterns of (a) Cu(001), (b)–(d) 4–12-ML Fe<sub>50</sub>Mn<sub>50</sub>/3-ML Co/3-ML Fe/Cu(001), (e) 3-ML Co/3-ML Fe/Cu(001), and (f)–(h) 4–12-ML Mn/3-ML Co/3-ML Fe/Cu(001) films, measured at 110 eV and 300 K.

were made under remanent conditions; these were generated by applying either a positive or negative external magnetic field ( $\pm 1000$  Oe) along the out-of-plane direction of the magnetic samples before placing them in the PEEM sample holder.

### III. RESULTS

#### A. Crystalline structure of $\text{Fe}_{50}\text{Mn}_{50}$ and Mn films on 3-ML Co/3-ML Fe/Cu(001)

The crystalline structures of  $\text{Fe}_{50}\text{Mn}_{50}$  and Mn films grown on 3-ML Co/3-ML Fe/Cu(001) were characterized using LEED. Figures 2(a)–2(h) display selected LEED patterns of Cu(001), 3-ML Co/3-ML Fe films, and 4–12-ML  $\text{Fe}_{50}\text{Mn}_{50}$  or 4–12-ML Mn films grown on 3-ML Co/3-ML Fe bilayers;

these patterns were measured at 110 eV. We observed that the  $p(1 \times 1)$  spots of these films were located at the same positions as those of Cu(001), indicating an epitaxial growth condition. Therefore, the in-plane lattice constants ( $a_{\parallel}$ ) of the  $\text{Fe}_{50}\text{Mn}_{50}$ , Mn, and 3-ML Co/3-ML Fe films were determined to be equal to that of Cu(001) (approximately 3.61 Å). For the  $\text{Fe}_{50}\text{Mn}_{50}$  film grown on 3-ML Co/3-ML Fe/Cu(001), we did not observe additional LEED spots associated with the formation of an ordered alloy; hence, we conclude that the prepared  $\text{Fe}_{50}\text{Mn}_{50}$  layers were chemically disordered crystalline films, a result that is in agreement with those of previous studies [18,35,36].

Figures 3(a) and 3(b) present the averaged interlayer distance ( $d_{\perp}$ ) values observed for  $\text{Fe}_{50}\text{Mn}_{50}$  and Mn films grown on 3-ML Co/3-ML Fe bilayers; these values were

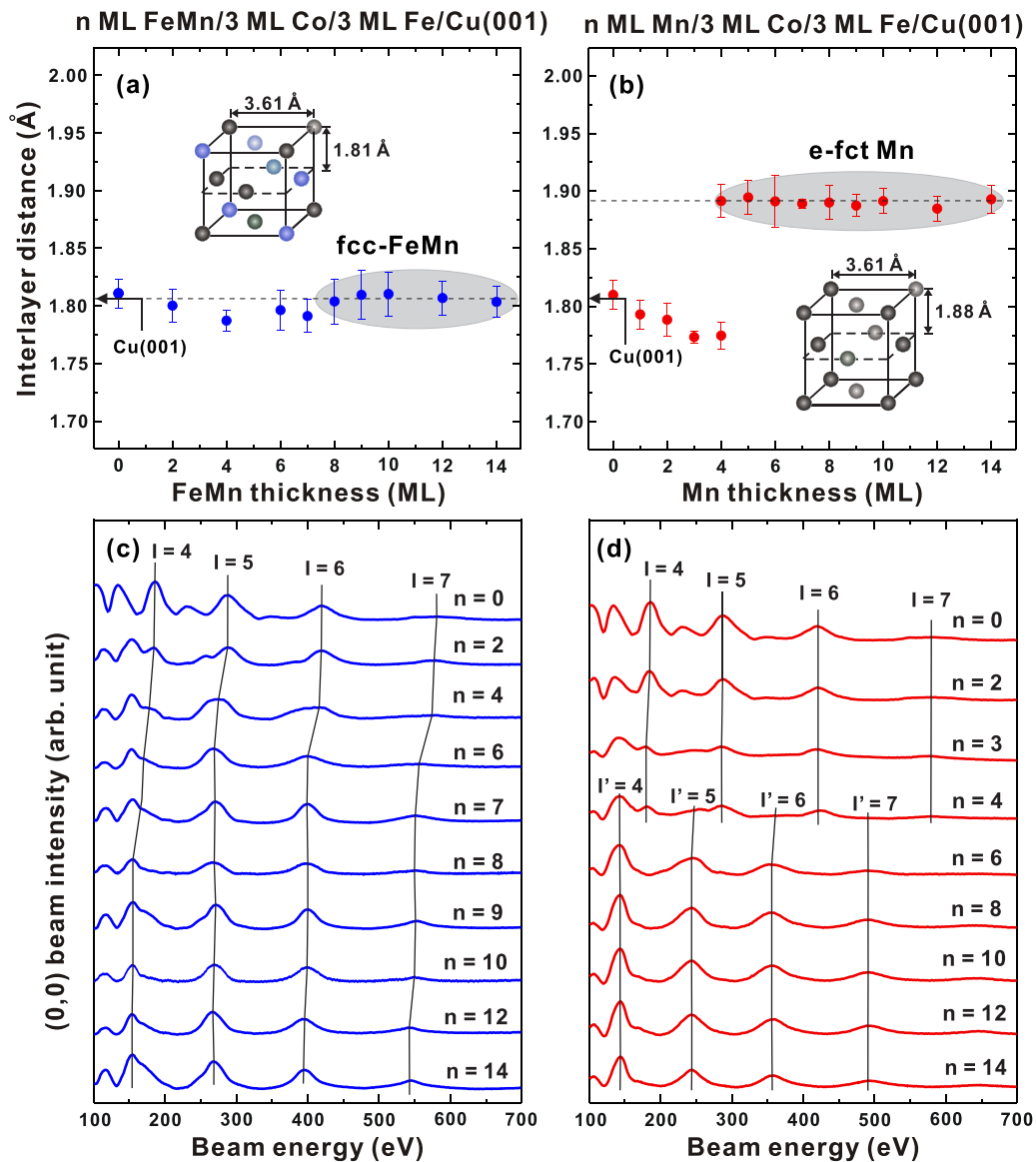


FIG. 3. Average interlayer distance ( $d_{\perp}$ ) of various (a)  $\text{Fe}_{50}\text{Mn}_{50}$  and (b) Mn films grown on 3-ML Co/3-ML Fe/Cu(001), as calculated according to the energy peaks ( $I$  or  $I'$ ) of the corresponding LEED specular spot  $I/V$  curves of panels (c) and (d) measured at 300 K. In panel (a),  $\text{Fe}_{50}\text{Mn}_{50}$  films grown on 3-ML Co/3-ML Fe/Cu(001) exhibit a fcc structure when  $t_{\text{FeMn}}$  exceeded 8 ML. In panel (b), Mn films grown on 3-ML Co/3-ML Fe/Cu(001) exhibit an e-fct structure transition when  $t_{\text{Mn}}$  exceeded 4 ML. In panels (a) and (b), the arrows represent  $d_{\perp}$  of Cu(001). The illustrations display the atomic model of the fcc  $\text{Fe}_{50}\text{Mn}_{50}$  and e-fct Mn films.

calculated according to the LEED  $I/V$  curves obtained from LEED specular spots [Figs. 3(c) and 3(d)]. The  $d_{\perp}$  values of the 3-ML Co/3-ML Fe/Cu(001) films were approximately 1.81 Å; this value is close to the previously reported value for fcc Co/Cu(001) films [37–40]. The  $d_{\perp}$  value of Fe<sub>50</sub>Mn<sub>50</sub> film at the early stage of growth on the 3-ML Co/3-ML Fe bilayers was slightly below 1.80 Å and then stabilized at the  $d_{\perp}$  of Cu(001) (1.81 Å) when the thickness of Fe<sub>50</sub>Mn<sub>50</sub> ( $t_{\text{FeMn}}$ ) reached 8 ML. Because of a finding of equal value for the vertical and in-plane lattice constants (i.e., the  $c/a \approx 1$ ), a formation of a stable fcc structure for those Fe<sub>50</sub>Mn<sub>50</sub> films when  $t_{\text{FeMn}} > 8$  ML can be concluded; this result is consistent with a previous experimental report [36]. On the other hand, the Mn films grown on 3-ML Co/3-ML Fe/Cu(001) had an fct structure if the thickness ( $t_{\text{Mn}}$ ) exceeded 4 ML [Fig. 3(b)]; this is similar to the behaviors of Mn films grown on 1-ML Fe<sub>50</sub>Mn<sub>50</sub>/3-ML Co/3-ML Fe/Cu(001) detailed in the Supplemental Material [27]. Our structural characterizations of the Fe<sub>50</sub>Mn<sub>50</sub> and Mn films are consistent with the results of previous studies [16,41].

### B. Magnetic properties of Fe<sub>50</sub>Mn<sub>50</sub>/3-ML Co/3-ML Fe films at room temperature

Figure 4(a) displays the magnetic hysteresis loops of the 0- to 10-ML Fe<sub>50</sub>Mn<sub>50</sub>/3-ML Co/3-ML Fe films measured at 300 K; the curves indicate that the magnetic anisotropy of a 3-ML Co/3-ML Fe film was originally in-plane oriented. When  $t_{\text{FeMn}} > 8$  ML, the magnetic anisotropy of the Fe<sub>50</sub>Mn<sub>50</sub>/3-ML Co/3-ML Fe films changed from the

in-plane to the out-of-plane direction. The onset of long-range AFM ordering of the Fe<sub>50</sub>Mn<sub>50</sub> film must be determined to clarify the correlation between the induced PMA and the antiferromagnetism of the Fe<sub>50</sub>Mn<sub>50</sub> in the Fe<sub>50</sub>Mn<sub>50</sub>/3-ML Co/3-ML Fe films. Examination of the long-range AFM order of the metallic AFM Fe<sub>50</sub>Mn<sub>50</sub> (or Mn) films through the acquisition of x-ray magnetic linear dichroism spectra [42–45] was hindered by the fixed orientation between the x-ray and the sample holder as well as by full magnetic shielding in the sample holder of the PEEM [34]. Therefore, we characterized the onset of long-range AFM ordering of the AFM films by observing the enhanced coercivity ( $H_c$ ) engendered in AFM/FM coupled systems; this approach has been justified in previous studies [10,35,36,46]. As illustrated in Fig. 4(c), the  $H_c$  value was substantially enhanced when  $t_{\text{FeMn}}$  exceeded 8 ML, indicating a threshold thickness of 8 to 9 ML for establishing long-range AFM ordering of the Fe<sub>50</sub>Mn<sub>50</sub> films. Notably, this threshold thickness is close to the critical  $t_{\text{FeMn}}$  for the onset of PMA [Fig. 4(b)], indicating that PMA induction in Fe<sub>50</sub>Mn<sub>50</sub>/3-ML Co/3-ML Fe and the establishment of antiferromagnetism in the Fe<sub>50</sub>Mn<sub>50</sub> films occurred simultaneously. This suggests that PMA could be triggered by the AFM Fe<sub>50</sub>Mn<sub>50</sub> film through AFM-FM exchange coupling.

The origin of the PMA induced in the Fe<sub>50</sub>Mn<sub>50</sub>/3-ML Co/3-ML Fe films was revealed through the XMCD measurements. Regarding the 10-ML Fe<sub>50</sub>Mn<sub>50</sub>/3-ML Co/3-ML Fe film, the Co, Fe, and Mn elements revealed similar XMCD asymmetries at the  $L_{3,2}$  edges [Figs. 5(a)–5(c)]; this indicates a parallel-like orientation of coupling between the Co moments and the uncompensated Mn moments at the

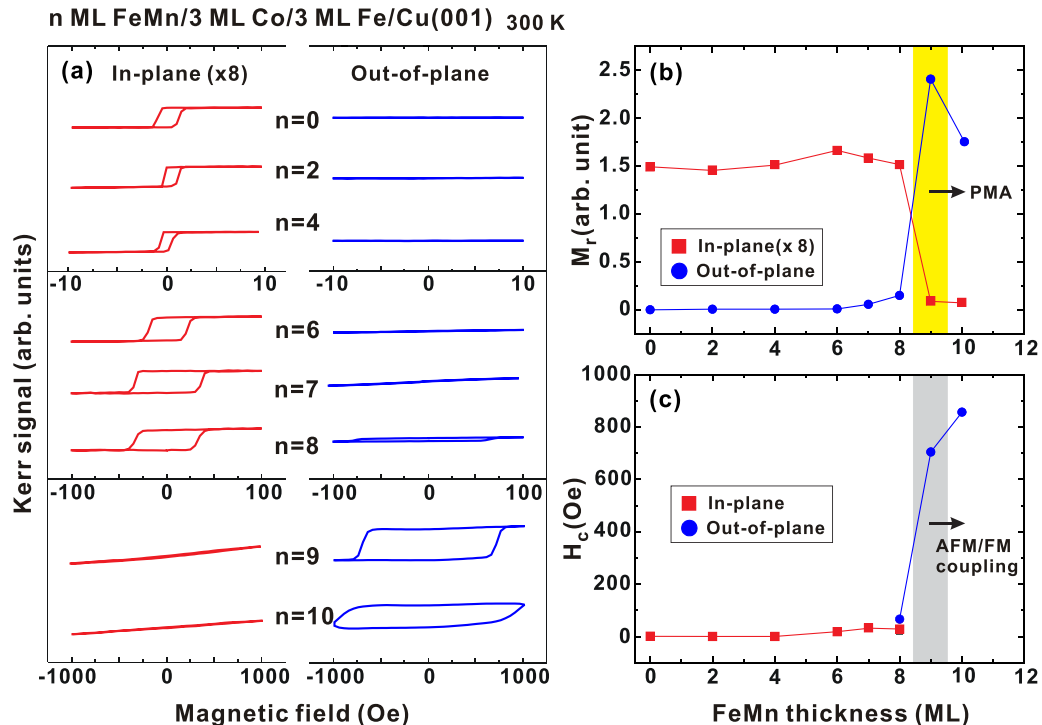


FIG. 4. (a) Magnetic hysteresis loops, (b)  $M_r$ , and (c)  $H_c$  of 0- to 10-ML Fe<sub>50</sub>Mn<sub>50</sub>/3-ML Co/3-ML Fe/Cu(001) measured at 300 K. In panel (b), the yellow shadow indicates the estimated critical thickness for the onset of PMA. In panel (c), the gray shadow indicates the estimated critical thickness for the onset of long-range AFM ordering in the Fe<sub>50</sub>Mn<sub>50</sub> film.

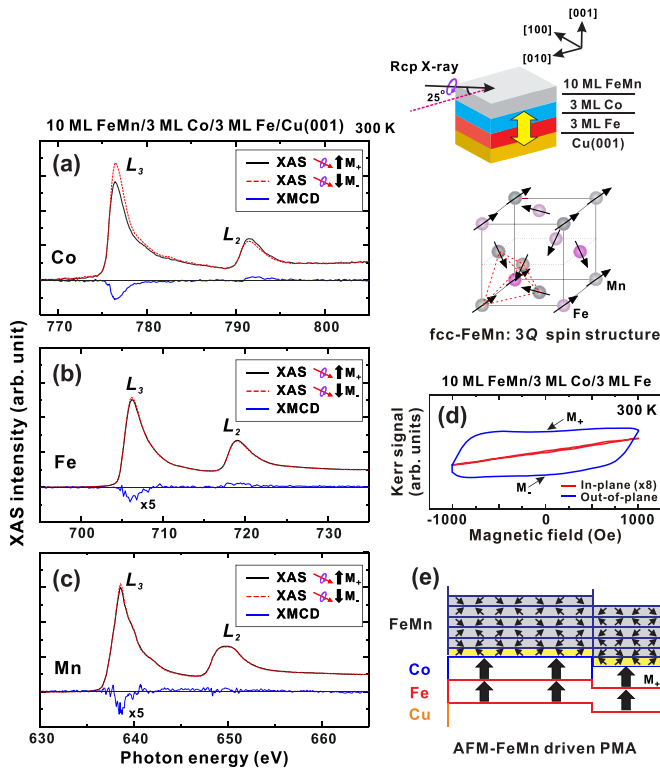


FIG. 5. XAS and XMCD curves of 10-ML  $\text{Fe}_{50}\text{Mn}_{50}$ /3-ML  $\text{Co}/3\text{-ML Fe}/\text{Cu}(001)$  measured at the (a) Co, (b) Fe, and (c) Mn  $L_{3,2}$  edges in the remanent states at 300 K. (d) Magnetic hysteresis loops of 10-ML  $\text{Fe}_{50}\text{Mn}_{50}$ /3-ML  $\text{Co}/3\text{-ML Fe}/\text{Cu}(001)$  measured by MOKE at 300 K. (e) Schematic illustration of the interfacial spin structure of  $\text{Fe}_{50}\text{Mn}_{50}$  coupled with the FM moments. The bold black arrows displayed in each figure indicate the remanent states of the films ( $M_+$  or  $M_-$ ) under positive or negative out-of-plane-oriented magnetic fields ( $\pm 1000$  Oe). The illustrations in the top-right of the figure show the geometry of the XMCD measurement [34] and the 3Q spin structure of the AFM  $\text{Fe}_{50}\text{Mn}_{50}$  film [18–21].

AFM/FM interface. According to the MOKE hysteresis loops [Fig. 5(d)], the magnetization of the 10-ML  $\text{Fe}_{50}\text{Mn}_{50}$ /3-ML  $\text{Co}/3\text{-ML Fe}$  film can only be flipped by the magnetic field along the out-of-plane direction ( $\pm 1000$  Oe). This indicates an established PMA as well as a large out-of-plane component of the magnetic moments in the 10-ML  $\text{Fe}_{50}\text{Mn}_{50}$ /3-ML  $\text{Co}/3\text{-ML Fe}$  film; the Co, Fe, and Mn XMCD signal in Figs. 5(a)–5(c) should be mainly contributed by the flipping of the Co, Fe, and uncompensated Mn moments along the out-of-plane direction. Thus, the finding of a FM-like coupling of the Fe, Co, and uncompensated Mn moments along the out-of-plane direction suggests an established collinearlike exchange coupling at the AFM-FM interface of the perpendicularly magnetic 10-ML  $\text{Fe}_{50}\text{Mn}_{50}$ /3-ML  $\text{Co}/3\text{-ML Fe}$  film [Fig. 5(e)]. In addition, as detailed in the Supplemental Material [27], the XMCD contrast of the Mn element in the in-plane magnetic 6-ML  $\text{Fe}_{50}\text{Mn}_{50}$ /3-ML  $\text{Co}/3\text{-ML Fe}$  film [Fig. S3(f)] is much weaker than that in the perpendicularly magnetic 10-ML  $\text{Fe}_{50}\text{Mn}_{50}$ /3-ML  $\text{Co}/3\text{-ML Fe}$  film [Figs. 5(c) and S3(c)]. This finding suggests that the interface spin structure of AFM  $\text{Fe}_{50}\text{Mn}_{50}$  films has a large out-of-plane component, but a smaller (or compensated) in-plane compo-

nent, which agrees with the 3Q-type AFM spin ordering of the  $\text{Fe}_{50}\text{Mn}_{50}$  film [illustration of Fig. 5] [18–21].

### C. Magnetic properties of Mn/(1-ML $\text{Fe}_{50}\text{Mn}_{50}$ )/3-ML $\text{Co}/3\text{-ML Fe}$ films at room temperature

Another possible PMA induction presented in this paper is in Mn/(1-ML  $\text{Fe}_{50}\text{Mn}_{50}$ )/3-ML  $\text{Co}/3\text{-ML Fe}$  films. Figure 6(a) displays the magnetic hysteresis loops of the 0- to 6-ML Mn/3-ML  $\text{Co}/3\text{-ML Fe}$  films measured at 300 K. When  $t_{\text{Mn}} > 4$  ML, the in-plane magnetization of the Mn/3-ML  $\text{Co}/3\text{-ML Fe}$  films decreased considerably. This indicates that the magnetization of the Mn/3-ML  $\text{Co}/3\text{-ML Fe}$  films with  $t_{\text{Mn}} > 4$  ML could not reach saturation under the current magnetic field ( $\leq 1000$  Oe); this behavior can be attributed to a slightly tilted magnetization or a considerable enhancement of  $H_c$  caused by Mn-induced AFM coupling [47]. After we incorporated a 1-ML  $\text{Fe}_{50}\text{Mn}_{50}$  film between the Mn and 3-ML  $\text{Co}/3\text{-ML Fe}$  films, however, PMA was triggered when  $t_{\text{Mn}}$  reached 5 ML [Fig. 6(b)]. According to Figs. 6(f) and 6(g), the appearance of PMA in the Mn/1-ML  $\text{Fe}_{50}\text{Mn}_{50}$ /3-ML  $\text{Co}/3\text{-ML Fe}$  film was accompanied by a significant increase in the perpendicular  $H_c$  value when  $t_{\text{Mn}} > 4$  ML, the thickness close to the onset of long-range AFM ordering in the Mn film. This indicates that the PMA established in the Mn/1-ML  $\text{Fe}_{50}\text{Mn}_{50}$ /3-ML  $\text{Co}/3\text{-ML Fe}$  films was not only affected by 1-ML  $\text{Fe}_{50}\text{Mn}_{50}$  at the interface but also originated from the exchange coupling induced by the full AFM Mn film; adding a 1-ML  $\text{Fe}_{50}\text{Mn}_{50}$  interfacial layer substantially changed the coupling orientation across the Mn-Co interface, even though no intrinsic AFM order for the 1-ML  $\text{Fe}_{50}\text{Mn}_{50}$  layer alone was expected. As presented in Fig. 4, applying the  $\text{Fe}_{50}\text{Mn}_{50}$  film with an out-of-plane-oriented spin component at the interface [Fig. 5] triggered robust PMA in the 3-ML  $\text{Co}/3\text{-ML Fe}$  films. Therefore, we inferred that the 1-ML  $\text{Fe}_{50}\text{Mn}_{50}$  film may still preserve out-of-plane spin components at the Mn-Co interface caused by magnetic proximity effects from adjacent Mn or Co moments [35]; these interfacial moments could help stabilize the PMA of the underlying 3-ML  $\text{Co}/3\text{-ML Fe}$  films when they were coupled with the in-plane-oriented Mn moments in the volume of the Mn film [22,23].

### D. Establishment of PMA in Mn/2-, 3-ML $\text{Co}/3\text{-ML Fe}$ films at low temperature

To explore other conditions for triggering PMA of the Mn/3-ML  $\text{Co}/3\text{-ML Fe}$  films, we performed MOKE measurements in a lower-temperature regime. Figure 6(c) presents that the 3-ML  $\text{Co}/3\text{-ML Fe}$  film exhibited also in-plane magnetic anisotropy at 155 K. However, the PMA of the Mn/3-ML  $\text{Co}/3\text{-ML Fe}$  films was generated when  $t_{\text{Mn}} > 4$  ML. As illustrated in Figs. 6(h) and 6(i), the stable perpendicular magnetization of the Mn/3-ML  $\text{Co}/3\text{-ML Fe}$  films was accompanied by a strong  $H_c$  enhancement. This is similar to the behavior observed in the Mn/1-ML  $\text{Fe}_{50}\text{Mn}_{50}$ /3-ML  $\text{Co}/3\text{-ML Fe}$  films at 300 K [Fig. 6(b)]. Furthermore, the evolution of PMA established in the Mn/3-ML  $\text{Co}/3\text{-ML Fe}$  films was traced through temperature-dependent measurements. As presented in Figs. 7(a)–7(c), the 4- to 8-ML Mn/3-ML  $\text{Co}/3\text{-ML Fe}$  films exhibited perpendicular

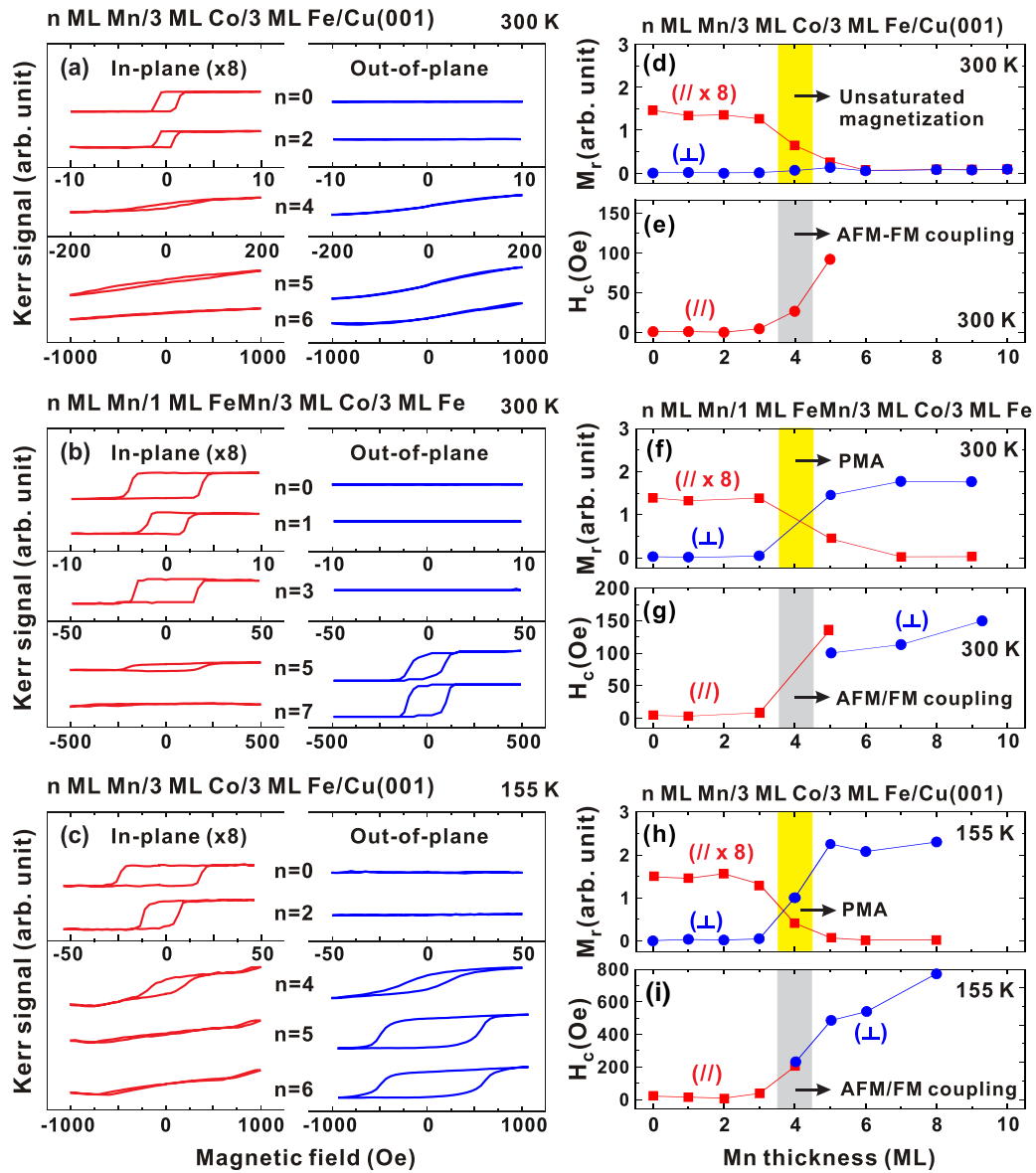


FIG. 6. Magnetic hysteresis loops of (a) 0- to 6-ML Mn/3-ML Co/3-ML Fe/Cu(001) and (b) 0- to 7-ML Mn/1-ML Fe<sub>50</sub>Mn<sub>50</sub>/3-ML Co/3-ML Fe/Cu(001) measured at 300 K. (c) Magnetic hysteresis loops of 0- to 6-ML Mn/3-ML Co/3-ML Fe/Cu(001) films measured at 155 K. (d)–(i) Summarized  $M_r$  and  $H_c$  values based on panels (a)–(c). In panel (d), the yellow shadow indicates the estimated critical thickness for the onset of unsaturated magnetization at 300 K. In panels (f) and (h), the yellow shadows indicate the estimated critical thicknesses for the onset of PMA at 300 and 155 K, respectively. In panels (e), (g), and (i), the gray shadows indicate the estimated critical thicknesses for the onset of an established long-range AFM ordering of Mn films at 300 or 155 K.

magnetization at low temperatures. However, PMA and  $H_c$  substantially decreased with elevated temperature. As detailed in the Supplemental Material [27], the  $d_{\perp}$  of the 6- and 8-ML e-fct Mn films grown on 3-ML Co/3-ML Fe/Cu(001) changed very little (from 1.88 to 1.86 Å) as the temperature decreased from 300 to 180 K. Therefore, the discovery that the magnetic anisotropy of the e-fct Mn/3-ML Co/3-ML Fe film changed substantially when the temperature was lower than 190 K should not be attributed to a sudden structural transformation of the Mn film.

To clarify why the PMA of the Mn/3-ML Co/3-ML Fe film was enhanced at low temperature, we initially investigated the capping effects generated by a thin Mn film at the

interface. Because the in-plane magnetic anisotropy of the 2-ML Co/3-ML Fe film was much lower than that of the 3-ML Co/3-ML Fe film [25], the interface effect caused by Mn could be detected at a higher sensitivity. Therefore, the measurements were conducted on Mn/2-ML Co/3-ML Fe film. As displayed in the upper portion of Fig. 7(d), the 2-ML Co/3-ML Fe film also exhibited stable in-plane magnetic anisotropy at 155–300 K. However, the PMA of the 1-ML Mn/2-ML Co/3-ML Fe film [lower portion of Fig. 7(d)] was enhanced for temperatures lower than 190 K. This indicates that the interfacial Mn layer contributed to PMA in the adjacent FM film when the temperature was reduced. Indeed, the promotion of perpen-

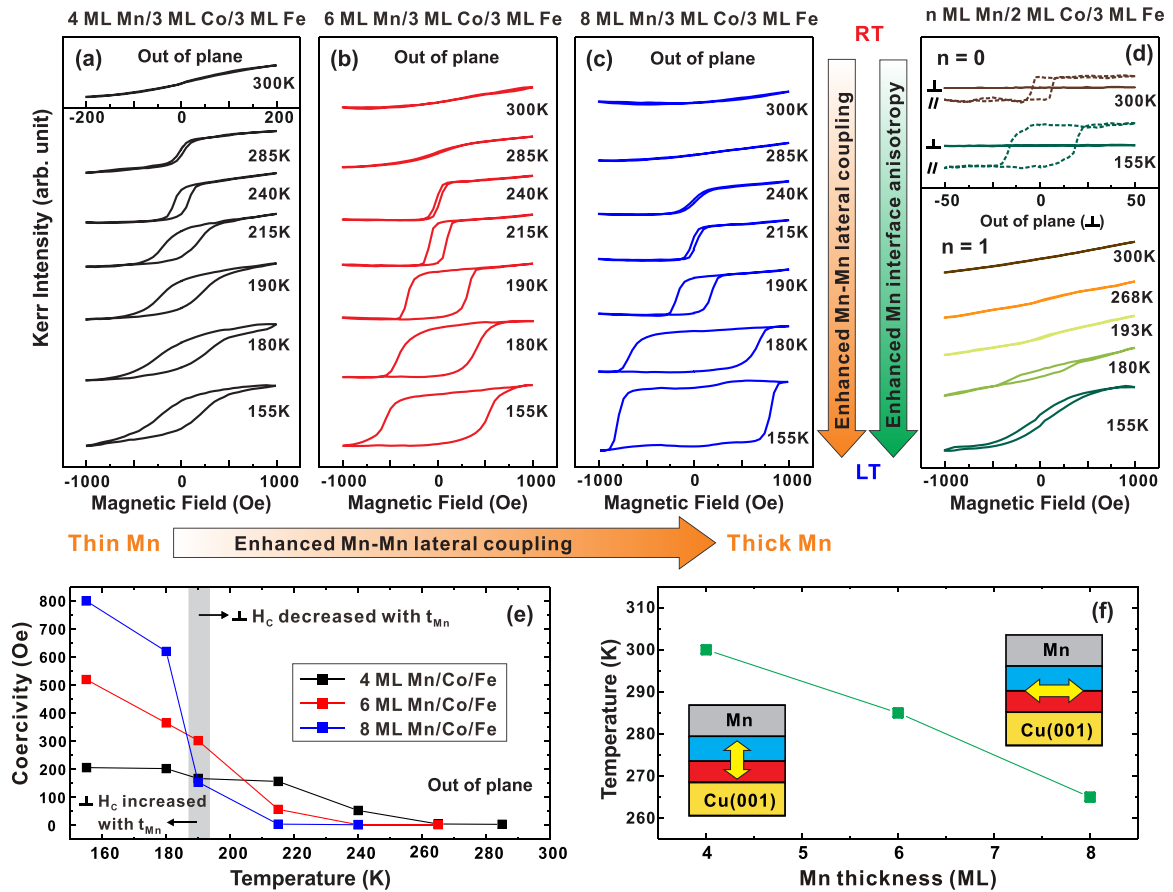


FIG. 7. (a)–(c) Perpendicular magnetic hysteresis loops of 4- to 8-ML Mn/3-ML Co/3-ML Fe/Cu(001) measured at various temperatures. (d) Perpendicular (solid line) and in-plane (dashed line) magnetic hysteresis loops of 0-, 1-ML Mn/2-ML Co/3-ML Fe/Cu(001) measured at various temperatures. (e) Summarized  $H_c$  values based on panels (a)–(c). (f) Critical temperatures for the absence of induced PMA in 4- to 8-ML Mn/3-ML Co/3-ML Fe/Cu(001). In the lower portion of panel (d), a presence of perpendicular magnetic hysteresis loops at low temperature is attributable to enhanced perpendicular interface anisotropy of the interfacial Mn moments in 1-ML Mn/2-ML Co/3-ML Fe/Cu(001). In panel (e), thickening  $t_{Mn}$  in Mn/3-ML Co/3-ML Fe/Cu(001) resulted in an increased perpendicular  $H_c$  when  $T < 190$  K but a reduced perpendicular  $H_c$  when  $T > 190$  K.

dicular crystalline anisotropy of the interfacial Mn moments through orbital hybridization at the interface has been observed in Mn/Co/Ni and NiMn/Mn/Co/Ni systems at 300 K [16,24]. We speculate that this effect could be further promoted at low temperatures through improved crystalline ordering and band narrowing at the interface [48–51]. According to the present results [lower portion of Fig. 7(d)] and literature [25], the perpendicular interface anisotropy value contributed by 1 ML Mn when the temperature lower than 190 K was enhanced to be  $\approx 1$  mJ/m<sup>2</sup> [27]. Thus, through an interplay of exchange coupling with the Mn moments in the volume of the Mn film, in Figs. 7(a)–7(c), the enhanced perpendicular interface anisotropy of the interfacial Mn moments could also help trigger PMA in the Mn/3-ML Co/3-ML Fe films at low temperatures; this is similar to the roles of 1-ML Fe<sub>50</sub>Mn<sub>50</sub> in triggering the PMA of the Mn/1-ML Fe<sub>50</sub>Mn<sub>50</sub>/3-ML Co/3-ML Fe film at 300 K [Fig. 6(b)].

To further examine the interface coupling in the Mn/3-ML Co/3-ML Fe film with induced PMA, the Co, Fe, Mn  $L_{3,2}$  XAS, and XMCD curves of a 6-ML Mn/3-ML Co/3-ML Fe film were measured at 100 K. As displayed in Figs. 8(a)–8(c), Fe and Co had distinguishable

XMCD asymmetry. However, no XMCD contrast was detected for the Mn element, even though a distinct perpendicular magnetization was observed by MOKE at low temperature ( $T < 190$  K) [Fig. 8(d)]. This result suggests that, under the out-of-plane magnetic fields, the flip of the out-of-plane component of the uncompensated Mn moments in the perpendicularly magnetic Mn/3-ML Co/3-ML Fe film is much smaller than that in the perpendicularly magnetic Fe<sub>50</sub>Mn<sub>50</sub>/3-ML Co/3-ML Fe film; the coupling orientation between the uncompensated Mn and FM moments in perpendicularly magnetic Mn/3-ML Co/3-ML Fe film [Fig. 8(e)] may be different from the collinearlike coupling present in perpendicularly magnetic Fe<sub>50</sub>Mn<sub>50</sub>/3-ML Co/3-ML Fe film [Fig. 5(e)]. However, examination of the in-plane component of the interfacial uncompensated Mn moments of the 6-ML Mn/3-ML Co/3-ML Fe film when  $T > 190$  K through the acquisition of XMCD was hindered by a huge in-plane  $H_c$  value ( $> 1000$  Oe) [Fig. 6(a)]. Hence, we inferred the in-plane component of the interfacial Mn moments from a similar system of the in-plane magnetic Mn/Co/Cu(001). In the past, the measurements of spin-polarized scanning tunneling microscopy had verified an in-plane layered-AFM

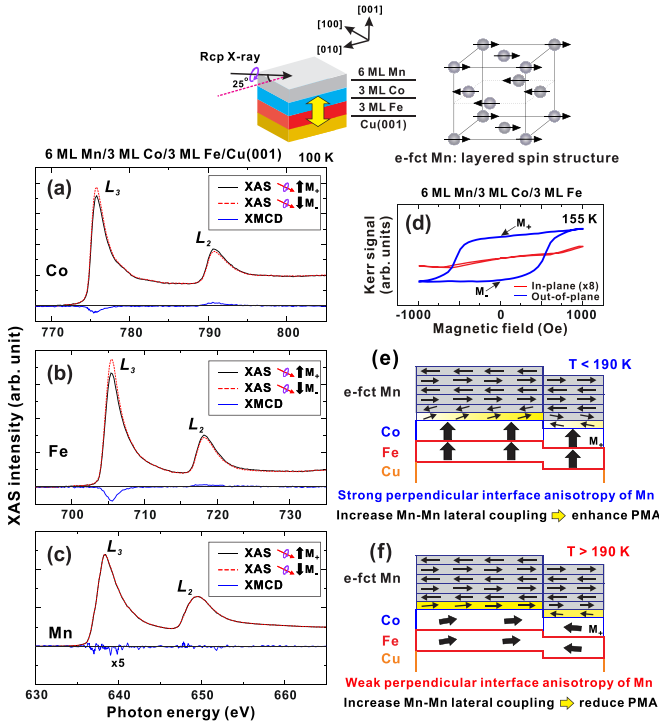


FIG. 8. XAS and XMCD curves of 6-ML Mn/3-ML Co/3-ML Fe/Cu(001) measured at the (a) Co, (b) Fe, and (c) Mn  $L_{3,2}$  edges in the remanent states at 100 K. (d) Magnetic hysteresis loops of 6-ML Mn/3-ML Co/3-ML Fe/Cu(001) measured by MOKE at 155 K. (e) and (f) Schematic illustrations of the magnetic configurations in Mn/3-ML Co/3-ML Fe/Cu(001) in low-temperature ( $T < 190$  K) and high-temperature regimes ( $T > 190$  K). The bold black arrows displayed in each figure indicate the remanent states of the films ( $M_+$  or  $M_-$ ) under positive or negative out-of-plane-oriented magnetic fields ( $\pm 1000$  Oe). The illustrations in the top part of the figure show the geometry of the XMCD measurement [34] and the in-plane layered AFM spin structure of the e-fct Mn film [22,23].

spin structure for the top layer of the Mn/Co/Cu(001) [22,23]. However, no Mn XMCD signal was detected in an in-plane magnetic Mn/Co/Cu(001) [52,53]. These results indicate that the interfacial uncompensated Mn moments in the in-plane magnetic Mn/Co/Cu(001) could have a highly frustrated in-plane component, which has been attributed to an effect of strong Mn-Mn lateral exchange coupling under the presence of interface or surface steps [54]. Therefore, combining the previous results and the current study yields a picture that the interfacial uncompensated Mn moments in the perpendicularly magnetic 6-ML Mn/3-ML Co/3-ML Fe film may have a highly frustrated in-plane component but a small uncompensated out-of-plane component which is contributed by the promoted perpendicular interface crystalline anisotropy at low temperature [Fig. 7(d)]. We speculated that these interfacial Mn moments may couple noncollinearly with the adjacent Co/Fe layers, triggering the establishment of PMA on the Mn/Co/Fe/Cu(001) system at low temperature [Fig. 8(e)]. Interestingly, as mentioned, the Mn XMCD signal in the Fe<sub>50</sub>Mn<sub>50</sub>/3-ML Co/3-ML Fe film with induced PMA was still preserved under the similar conditions of interface or substrate steps [Fig. 5(c)]. We

speculated that this may be attributed to a lower strength lateral (but higher strength out-of-plane oriented) exchange coupling in the 3Q spin structure of AFM Fe<sub>50</sub>Mn<sub>50</sub> [18–21].

#### IV. DISCUSSION

##### Characteristic behaviors and exchange-coupling mechanisms for the Fe<sub>50</sub>Mn<sub>50</sub>- and Mn-induced PMA in Co/Fe films with strong in-plane magnetic anisotropy

According to the aforementioned results [Figs. 5(a)–5(c)], Co, Fe, and Mn had distinguishable XMCD asymmetry in the perpendicularly magnetic Fe<sub>50</sub>Mn<sub>50</sub>/3-ML Co/3-ML Fe film. This confirms a FM-like ordering or collinearlike exchange coupling of the Co, Fe, and uncompensated Mn moments with an out-of-plane component at the AFM-FM interface of the perpendicularly magnetic Fe<sub>50</sub>Mn<sub>50</sub>/3-ML Co/3-ML Fe film [Fig. 5(e)]. Furthermore, the strength of the induced PMA, as well as the value of perpendicular  $H_c$  in the Fe<sub>50</sub>Mn<sub>50</sub>/3-ML Co/3-ML Fe films can be greatly increased by thickening  $t_{\text{FeMn}}$  [Fig. 4]. This behavior accords with the finite-size tendency of the AFM-induced exchange coupling [17] and demonstrates a characteristic of “collinearlike exchange-coupling”-facilitated PMA in the Fe<sub>50</sub>Mn<sub>50</sub>/3-ML Co/3-ML Fe films. By contrast, according to Figs. 7(a)–7(c) and 7(e), the PMA of Mn/3-ML Co/3-ML Fe films behaved nontrivial  $t_{\text{Mn}}$ -dependent tendencies at different temperature regimes. At low temperatures ( $T < 190$  K), increasing  $t_{\text{Mn}}$  resulted in an enhanced perpendicular  $H_c$  [Fig. 7(e)]; this might be due to increased domain-wall-activated processes caused by competition between the enhanced in-plane-oriented lateral Mn-Mn exchange coupling and the established perpendicular crystalline anisotropy of the interfacial Mn moments [Fig. 8(e)] [9,46,54]. By contrast, if  $T > 190$  K, increasing  $t_{\text{Mn}}$  merely reduced the perpendicular  $H_c$  and the thermal stability of PMA of the Mn/3-ML Co/3-ML Fe films [Figs. 7(e) and 7(f)]; this might have resulted from a weakened perpendicular crystalline anisotropy of the interfacial Mn moments when  $T > 190$  K [Fig. 7(d)] and the dominant effects of the in-plane-oriented lateral Mn-Mn exchange coupling with an increase in  $t_{\text{Mn}}$  [Fig. 8(f)]. Thus, the characteristic nontrivial  $t_{\text{Mn}}$ -dependent PMA-induction behaviors, generated by a competition between the volume Mn and interface Mn moments in different temperature regimes, could provide a strong evidence for an established noncollinear exchange coupling at the AFM-FM interface of the perpendicularly magnetic Mn/3-ML Co/3-ML Fe films. Interestingly, such a behavior was clearly present in the Mn/3-ML Co/3-ML Fe films but not in the previous reported Mn/2-ML Co/14-ML Ni films [16,24]. We speculated that this may be attributed to a highly competitive relationship between the AFM-induced PMA and strong in-plane magnetic anisotropy of the FM film in the Mn/3-ML Co/3-ML Fe systems. Thus, through examination of the uncompensated Mn moments at the AFM-FM interface [Figs. 5(c) and 8(c)] and the characteristic behaviors of  $t_{\text{FeMn}}$  ( $t_{\text{Mn}}$ )-dependent magnetic anisotropy [Figs. 4 and 7] in the perpendicularly magnetic Fe<sub>50</sub>Mn<sub>50</sub>/3-ML Co/3-ML Fe and Mn/3-ML Co/3-ML Fe films, the present work has verified a similar exchange-coupling mechanism but different balances between competing couplings of the AFM and FM moments



in two systems. Furthermore, through an application of these mechanisms, Fe<sub>50</sub>Mn<sub>50</sub> and Mn/1-ML Fe<sub>50</sub>Mn<sub>50</sub> films are capable of stabilizing the PMA of a 3-ML Co/3-ML Fe film with strong in-plane magnetic anisotropy at room temperature [Figs. 4(a) and 6(b)]. Although a direct application of the proposed systems for the current perpendicular-based magnetic tunnel junctions may be limited by the unclarified issues of a structural compatibility of achieving bcc (MgO) and fcc Fe<sub>50</sub>Mn<sub>50</sub> (or e-fct Mn) electrodes and a diffusion of Mn upon thermal annealing, the findings here are important in understanding the mechanism and critical behaviors for antiferromagnet-induced PMA in ferromagnets with strong in-plane magnetic anisotropy.

## V. CONCLUSION

In conclusion, we examined the characteristic behavior, mechanisms, and critical conditions necessary for triggering PMA in Co/Fe films with strong in-plane magnetic anisotropy using AFM fcc Fe<sub>50</sub>Mn<sub>50</sub> and e-fct Mn films. Our results demonstrated that robust PMA in the

Co/Fe films can be generated by fcc Fe<sub>50</sub>Mn<sub>50</sub> films through collinearlike AFM-FM exchange coupling at room temperature. By contrast, the PMA triggered by the e-fct Mn film behaved a nontrivial Mn-dependent tendency at different temperature regimes; this originated from a competition between the out-of-plane-oriented moments at the interface and the in-plane-oriented Mn moments within the volume in an established noncollinear exchange coupling across the AFM-FM interface. Our findings provide the mechanism, characteristic behaviors, and practical conditions for increasing control over the PMA induction in FM films with a high magnetic moment density but large in-plane magnetic anisotropy, which is useful for the development of next-generation perpendicular spintronic devices that use AFM films to trigger PMA in FM films.

## ACKNOWLEDGMENTS

This work was partly supported by the Ministry of Science and Technology, Taiwan (Grant No. MOST 110-2112-M-018-007).

- 
- [1] S. Ikeda, K. Miura, H. Yamamoto, K. Mizunuma, H. D. Gan, M. Endo, S. Kanai, J. Hayakawa, F. Matsukura, and H. Ohno, *Nat. Mater.* **9**, 721 (2010).
- [2] D. C. Worledge, G. Hu, D. W. Abraham, J. Z. Sun, P. L. Trouilloud, J. Nowak, S. Brown, M. C. Gaidis, E. J. O'Sullivan, and R. P. Robertazzi, *Appl. Phys. Lett.* **98**, 022501 (2011).
- [3] S. Mangin, D. Ravelosona, J. A. Katine, M. J. Carey, B. D. Terris, and E. E. Fullerton, *Nat. Mater.* **5**, 210 (2006).
- [4] Y. Shiroishi, K. Fukuda, I. Tagawa, H. Iwasaki, S. Takenoiri, H. Tanaka, H. Mutoh, and N. Yoshikawa, *IEEE Trans. Magn.* **45**, 10 (2009).
- [5] N. Nakajima, T. Koide, T. Shidara, H. Miyauchi, H. Fukutani, A. Fujimori, K. Iio, T. Katayama, M. Nývlt, and Y. Suzuki, *Phys. Rev. Lett.* **81**, 5229 (1998).
- [6] M. T. Johnsony, P. J. H. Bloemenz, F. J. A. den Broeder, and J. J. de Vries, *Rep. Prog. Phys.* **59**, 1409 (1996).
- [7] T. Burkert, L. Nordström, O. Eriksson, and O. Heinonen, *Phys. Rev. Lett.* **93**, 027203 (2004).
- [8] A. Winkelmann, M. Przybylski, F. Luo, Y. Shi, and J. Barthel, *Phys. Rev. Lett.* **96**, 257205 (2006).
- [9] J. Stöhr and H. C. Siegmann, *Magnetism: From Fundamentals to Nanoscale Dynamics* (Springer, New York, 2006).
- [10] C. Won, Y. Z. Wu, H. W. Zhao, A. Scholl, A. Doran, W. Kim, T. L. Owens, X. F. Jin, and Z. Q. Qiu, *Phys. Rev. B* **71**, 024406 (2005).
- [11] Q. F. Zhan and K. M. Krishnan, *Appl. Phys. Lett.* **96**, 112506 (2010).
- [12] B. Y. Wang, N. Y. Jih, W. C. Lin, C. H. Chuang, P. J. Hsu, C. W. Peng, Y. C. Yeh, Y. L. Chan, D. H. Wei, W. C. Chiang, and M. T. Lin, *Phys. Rev. B* **83**, 104417 (2011).
- [13] P. Kuświk, P. L. Gastelois, M. M. Soares, H. C. N. Tolentino, M. De Santis, A. Y. Ramos, A. D. Lamirand, M. Przybylski, and J. Kirschner, *Phys. Rev. B* **91**, 134413 (2015).
- [14] P. Kuświk, B. Szymański, B. Anastaziak, M. Matczak, M. Urbaniak, A. Ehresmann, and F. Stobiecki, *J. Appl. Phys.* **119**, 215307 (2016).
- [15] B.-Y. Wang, M.-S. Tsai, C.-W. Huang, C.-W. Shih, C.-J. Chen, K. Lin, J.-J. Li, N.-Y. Jih, C.-I Lu, T.-H. Chuang, and D.-H. Wei, *Phys. Rev. B* **96**, 094416 (2017).
- [16] B.-Y. Wang, P.-H. Lin, M.-S. Tsai, C.-W. Shih, M.-J. Lee, C.-W. Huang, N.-Y. Jih, P.-Y. Cheng, and D.-H. Wei, *Phys. Rev. B* **92**, 214435 (2015).
- [17] T. Ambrose and C. L. Chien, *Phys. Rev. Lett.* **76**, 1743 (1996).
- [18] W. Kuch, L. I. Chelaru, F. Offi, J. Wang, M. Kotsugi, and J. Kirschner, *Phys. Rev. Lett.* **92**, 017201 (2004).
- [19] J. S. Kouvel and J. S. Kasper, *J. Phys. Chem. Solids* **24**, 529 (1963).
- [20] H. Umebayashi and Y. Ishikawa, *J. Phys. Soc. Jpn.* **21**, 1281 (1966).
- [21] M. Ekholm and I. A. Abrikosov, *Phys. Rev. B* **84**, 104423 (2011).
- [22] P.-J. Hsu, C.-I Lu, Y.-H. Chu, B.-Y. Wang, C.-B. Wu, L.-J. Chen, S.-S. Wong, and M.-T. Lin, *Phys. Rev. B* **85**, 174434 (2012).
- [23] C. B. Wu, J. Song, and W. Kuch, *Appl. Phys. Lett.* **101**, 012404 (2012).
- [24] B.-Y. Wang, C.-H. Hsiao, B.-X. Liao, C.-Y. Hsu, T.-H. Li, Y.-L. Hsu, Y.-M. Lai, M.-S. Tsai, T.-H. Chuang, and D.-H. Wei, *Phys. Rev. B* **104**, 024424 (2021).
- [25] J. Shen, A. K. Swan, and J. F. Wendelken, *Appl. Phys. Lett.* **75**, 2987 (1999).
- [26] The energy unit conversion for the magnetic anisotropy energy of Co/Fe/Cu(001) films is  $1 \text{ mJ/m}^2 \approx 0.4 \text{ meV/atom}$ .
- [27] See Supplemental Material at <http://link.aps.org/supplemental/10.1103/PhysRevB.105.184415> for the information of the crystalline structure of Mn/(1-ML FeMn)/3-ML Co/3-ML Fe/Cu(001), the calculation of the magnetic anisotropy energy of 2-, 3-ML Co/3-ML Fe/Cu(001) and 1-ML Mn/2-ML Co/3-

- ML Fe/Cu(001), and a comparison of XMCD of 6-, 10-ML Fe<sub>50</sub>Mn<sub>50</sub>/3-ML Co/3-ML Fe/Cu(001) films.
- [28] L. Néel, *C. R. Acad. Sci.* **237**, 1468 (1953); *J. Phys. Radium* **15**, 225 (1954).
- [29] B. Schulz and K. Baberschke, *Phys. Rev. B* **50**, 13467 (1994).
- [30] R. F. Willis, J. A. C. Bland, and W. Schwarzhacher, *J. Appl. Phys.* **63**, 4051 (1988).
- [31] B.-Y. Wang, C.-Y. Hsu, B.-X. Liao, Y.-L. Hsu, Y.-M. Lai, M.-S. Tsai, T.-H. Chuang, and D.-H. Wei, *Phys. Rev. B* **104**, 174407 (2021).
- [32] J. Stöhr, Y. Wu, B. D. Hermsmeier, M. G. Samant, G. R. Harp, S. Koranda, D. Dunham, and B. P. Tonner, *Science* **259**, 658 (1993).
- [33] C. M. Schneider and G. Schönhense, *Rep. Prog. Phys.* **65**, 1785 (2002).
- [34] D.-H. Wei, Y.-L. Chan, and Y.-J. Hsu, *J. Electron Spectrosc. Relat. Phenom.* **185**, 429 (2012).
- [35] K. Lenz, S. Zander, and W. Kuch, *Phys. Rev. Lett.* **98**, 237201 (2007).
- [36] F. Offi, W. Kuch, and J. Kirschner, *Phys. Rev. B* **66**, 064419 (2002).
- [37] O. Heckmann, H. Magman, P. le Fevre, D. Chandesris, and J. J. Rehr, *Surf. Sci.* **312**, 62 (1994).
- [38] J. R. Cerdá, P. L. de Andres, A. Cebollada, R. Miranda, E. Navas, P. Schuster, C. M. Schneider, and J. Kirschner, *J. Phys.: Condens. Matter* **5**, 2055 (1993).
- [39] W. Weber, A. Bischof, R. Allenspach, C. H. Back, J. Fassbender, U. May, B. Schirmer, R. M. Jungblut, G. Güntherodt, and B. Hillebrands, *Phys. Rev. B* **54**, 4075 (1996).
- [40] E. Navas, P. Schuster, C. M. Schneider, J. Kirschner, A. Cebollada, C. Ocal, R. Miranda, J. Cerdá, and P. de Andrés, *J. Magn. Magn. Mater.* **121**, 65 (1993).
- [41] J. T. Kohlhepp and W. J. M. de Jonge, *Phys. Rev. Lett.* **96**, 237201 (2006).
- [42] A. Scholl, J. Stöhr, J. Lüning, J. W. Seo, J. Fompeyrine, H. Siegart, J. P. Locquet, F. Nolting, S. Anders, E. E. Fullerton, M. R. Scheinfein, and H. A. Padmore, *Science* **287**, 1014 (2000).
- [43] H. Ohldag, A. Scholl, F. Nolting, S. Anders, F. U. Hillebrecht, and J. Stöhr, *Phys. Rev. Lett.* **86**, 2878 (2001).
- [44] W. Kim, E. Jin, J. Wu, J. Park, E. Arenholz, A. Scholl, C. Hwang, and Z. Q. Qiu, *Phys. Rev. B* **81**, 174416 (2010).
- [45] W. J. Antel, Jr., F. Perjeru, and G. R. Harp, *Phys. Rev. Lett.* **83**, 1439 (1999).
- [46] J. Nogués and I. K. Schuller, *J. Magn. Magn. Mater.* **192**, 203 (1999).
- [47] B.-Y. Wang, P.-H. Lin, M.-S. Tsai, C.-W. Shih, M.-J. Lee, C.-W. Huang, N.-Y. Jih, and D.-H. Wei, *Phys. Rev. B* **94**, 064402 (2016).
- [48] M. Kowalewski, C. M. Schneider, and B. Heinrich, *Phys. Rev. B* **47**, 8748 (1993).
- [49] W. C. Lin, C. C. Kuo, C. L. Chiu, and M.-T. Lin, *J. Appl. Phys.* **89**, 7139 (2001).
- [50] B.-Y. Wang, J.-Y. Hong, K.-H. O. Yang, Y.-L. Chan, D.-H. Wei, H.-J. Lin, and M.-T. Lin, *Phys. Rev. Lett.* **110**, 117203 (2013).
- [51] F. E. Gabaly, K. F. McCarty, A. K. Schmid, J. de la Figuera, M. C. Muñoz, L. Szunyogh, P. Weinberger, and S. Gallego, *New J. Phys.* **10**, 073024 (2008).
- [52] M. Caminale, R. Moroni, P. Torelli, W. C. Lin, M. Canepa, L. Mattera, and F. Bisio, *Phys. Rev. Lett.* **112**, 037201 (2014).
- [53] W. L. O'Brien and B. P. Tonner, *Phys. Rev. B* **50**, 2963 (1994).
- [54] B.-Y. Wang, J.-Y. Hong, N.-Y. Jih, K.-H. Ou Yang, L.-R. Chen, H.-J. Lin, Y.-L. Chan, D.-H. Wei, and M.-T. Lin, *Phys. Rev. B* **90**, 224424 (2014).